In Lecture Series on Numerical Optimization Methods & Tools for Multi-Criteria/Multi-Disciplinary Design with Applications to Aeronautics and Turbomachinery, Von Karman Institute for Fluid Dynamics, Belgium, Nov. 15 – 19, 2004.

AERO-THERMAL-ELASTICITY-MATERIALS OPTIMIZATION OF COOLED GAS TURBINE BLADES: PART I

G. S. Dulikravich*, T. J. Martin, B. H. Dennis*** and I. N. Egorov****

* Department of Mechanical and Materials Engineering, Florida International University, MAIDROC Laboratory, 10555 W. Flagler St., Miami, FL 33174, U.S.A.

** Pratt & Whitney Engine Company, Turbine Discipline Engineering & Optimization Group, M/S 169-20, East Hartford, CT 06108, U.S.A.

*** Department of Mechanical and Aerospace Engineering, University of Texas at Arlington, UTA Box 19018, 500 West First Street, Arlington, TX 76019, U.S.A.

**** IOSO Technology Center, Vekovaia St., 21, Office 203, 109544, Moscow, Russia

ABSTRACT

The first lecture in this two-lecture sequence provides background and general concepts. The second lecture provides practical examples. The objective of these two lectures is to provide a modular design optimization tool description that will take into account interaction of the hot gas flow-field, heat transfer in the blade material, internal coolant flow-field, stresses and deformations of the blades in a multi-stage axial gas turbine. These methodologies should result in a multi-disciplinary design optimization tool for the entire system (a multi-stage turbine) rather than a design method for an isolated component (a single turbomachinery blade). In order to make the entire design methodology computationally economical, the proposed method should utilize a combination of fast approximate models as well as highly accurate and detailed complete models for aerodynamics, heat transfer, and thermoelasticity. These calculations should be performed using parallel computing. The by-products of the optimization are shapes, optimized average surface roughness of the coolant passages, coolant bulk temperature variation, coolant bulk pressure variation and pressure losses in the coolant passages, and surface convective heat transfer coefficients in each of the coolant passages.

The resulting benefits of using this general approach to design are:

1. maximized efficiency and minimum size and weight of the entire multi-stage cooled gas turbine at design and a wide range of off-design conditions,
2. multi-stage 3-D analysis and design capability instead of an isolated blade row capability,
3. simultaneous account of aerodynamics, heat transfer, and thermoelasticity instead of aerodynamics alone,
4. ability to specify geometric, flow-field, thermal, and stress/deformation constraints,
5. capability to analyze and optimize thermally coated and uncoated turbine blades,
6. maximized turbine inlet temperature for a fixed coolant mass flow rate,
7. minimized coolant mass flow rate for a fixed turbine inlet temperature,
8. optimized average surface roughness of the internal coolant flow passage walls,
9. reduced need for manufacturing of small holes for blade film cooling,
10. optimized networking of the small cooling channels for transpiration cooling,
11. optimized blade shapes in each blade row for minimum total pressure loss and maximum torque,
12. optimized thickness distribution of blade walls and interior struts of coolant flow passages inside each blade row,
13. optimized concentrations of alloying elements to be used for the blade material,
14. minimized overall design cycle time.

In summary, the proposed multi-disciplinary design optimization method will provide the designer with a tool to guide him/her in the development of higher efficiency multi-stage axial gas turbines having internally cooled, thermally coated or non-coated blades that will cost less to manufacture, have a longer life span, be easier to repair, require less coolant, and sustain higher turbine inlet temperatures without contributing to air pollution.

1. INTRODUCTION

The greatest efficiency improvements in gas turbine engines are likely to be accomplished by enhancing the ability of turbine components to handle the highest possible centrifugal and thermal loads. Although higher speeds contribute to higher thrust-to-weight ratio and more compact engines, these lectures focus only upon thermal optimization of the turbine at a fixed rotor speed. This is because a proper determination of the engine performance with respect to the rotor speed is intrinsically related to a rigorous modeling of the compressor. On the other hand, the existence of high temperatures can result in plastic thermal strains, melting, oxidation, sulfidation, and environmentally contaminant nitrous oxide emissions. Higher rotational speeds create larger temperature drops, but also cause higher stresses and decreased life due to thermally enhanced creep. It is, therefore, very important in terms of engine performance and durability to sustain the highest possible temperatures in the turbine. Presently available materials, such as nickel-based alloys, cannot withstand metal temperatures in excess of 1300 K, but the turbine inlet gas temperatures can be increased by cooling the turbine blades. The incorporation of coolant and improvements in materials have resulted in increases in turbine inlet temperature from 850 K in 1960 to 1700 K today, with about 350 K attributed to the cooling devices alone [1]. Since a 1% increase in turbine inlet temperature can produce a 3% - 4% increase in engine output [2], cooling of turbine blades has been a major focus in modern gas turbines.

Although turbine cooling becomes more critical for high-speed aircraft, the jet engine specific thrust increases continuously with an increase in the turbine inlet temperature for all engine classifications, assuming all other variables such as flight Mach number and air mass flow rate are held constant. This performance relationship, as well as the thrust-specific fuel consumption's dependence upon turbine inlet temperature, are valid for turbojet, turbofan, turboprop, and industrial gas turbines [3]. The proportionality to specific fuel consumption is a little more complicated because higher temperatures allow greater power to be extracted by the turbine, and the optimum compressor pressure ratio is dependent upon that amount of power. Each compressor stage is already designed nearly at its operational limit as defined by the maximum stall pressure ratio, but this limit can be increased by increasing the rotor speed and temperature drop. Increased turbine inlet temperature can lead directly to a more compact engine with a smaller number of compressor stages. Thus, specific thrust and thrust-specific fuel consumption, as well as engine weight, can be optimized by increasing the turbine inlet gas temperature.

Modern turbomachinery rotor blades and vanes have traditionally been cooled by directing compressor bleed air through passages in the engine and into the complex serpentine-like coolant flow passages within the blades. The advantages of increasing the turbine inlet temperature are offset by the mechanical and manufacturing complexity of the cooling passages, as well as by the performance losses due to the bleeding of coolant air from the compressor to accomplish this task. Much of the cooling is accomplished through the convection on the internal coolant passage surfaces. Generally, the greater the coolant flow rate, the cooler the blade becomes. Advanced cooling schemes such as trip strips or turbulators, impingement cooling, and miniature heat exchangers can provide further enhancements to the magnitude of convection heat transfer, but they invariably result in even

greater pressure losses. Film cooling can produce a protective layer of cool air on the surface of the blades, but more cooling air must be bled from higher compressor stages in order to drive them. Moreover, film cooling especially at very high gas temperatures causes rapid increase in NOx and deteriorates the aerodynamic performance of the blade.

The aerospace engineer thus encounters the conflicting goals of the internal cooling optimization paradox. The heat transfer into the turbine blade should be maximized so that the turbine inlet temperature can be increased, which is contrary to the other objective of minimizing the coolant flow rate and the coolant pressure losses in the coolant passages. Simultaneously, the objective is to avoid extremely large temperature gradients in order to prevent thermal stresses and thermal barrier coating spalation.

Thus, the following question can be posed, ***"Is it possible to design a turbine cooling scheme that simultaneously maximizes the turbine inlet temperature, minimizes the coolant requirements, and maintains its structural integrity?"***

This article presents a methodology that proposes to answer this question positively. Each facet of the puzzle will be addressed in a tightly coupled multi-disciplinary fashion. Ultimately, an estimate of the real gas turbine efficiency, either specific thrust or thrust-specific fuel consumption, should be optimized given a flight Mach number, air intake, fuel flow rate, and fixed range of pressures available in the compressor. During the iterative numerical optimization process, the material and structural integrity of the blades will not be compromised. All of these optimization objectives and constraints should be incorporated into a realistic, aero-thermo-structural, internally cooled, thermal-barrier coated, turbine blade design system.

1.1. Global objectives

A linear combination of two important performance parameters of a gas turbine engine (specific thrust (thrust-to-mass flow rate of air, $T/\dot{m}_a a_0$) [4]

$$\frac{T}{\dot{m}_a a_0} = M_0 \left\{ \sqrt{\left(\frac{T_{01}/T_1}{T_{01}/T_1 - 1} \right) \left(\frac{T_{0t}/T_1}{(T_{01}/T_1)\pi_c^{1-1/\gamma}} - 1 \right) \left(\pi_c^{1-1/\gamma} - 1 \right) + \frac{T_{0t}/T_1}{(T_{01}/T_1)\pi_c^{1-1/\gamma}}} - 1 \right\} \tag{1}$$

and thrust-specific fuel consumption (mass flow rate of fuel per unit thrust, $\dot{m}_f/T$))

$$\frac{\dot{m}_f}{T} = \frac{c_p \left(T_{0t}/T_1 - (T_{01}/T_1)\pi_c^{1-1/\gamma} \right)}{Q_R \left(\frac{T}{\dot{m}_a} \right)} \tag{2}$$

should be optimized. The expressions for these parameters are given for an ideal turbojet. Here, M_0 is the flight Mach number, $\dot{m}_a$ is the air mass flow rate, $\dot{m}_f$ is the fuel consumption, a_o is the speed of sound, T_{0t} is the turbine inlet total temperature, T_{01} and T_1 are the total and static temperatures at the engine inlet, QR is the heat value of the fuel, and π_c is the compressor stagnation pressure rise ratio.

These expressions assume an isentropic engine, that is, adiabatic and frictionless, and without any mechanical losses or leaks. It also neglects the situation where air is bled from the compressor to drive the cooling flows in the combustor and turbine.

In turboshaft and high-bypass turbofan engines, the efficiency of internally cooled turbines is central to engine performance. There are four main sources of loss in a turbine; internal cooling losses, profile losses due to shock and boundary layer losses, secondary flow losses, and tip leakage losses. The turbine cooling air influences turbine efficiency in three ways. First, the cooling air emerging from the blades increases the drag. Second, the cooling air suffers a pressure loss in passing through the cooling passages, thus decreases π_t. Finally, the transfer of heat from the hot gases to the cooling flow increases the entropy. The effect of cooling the turbine modifies the definition for the turbine efficiency. This turbine efficiency is defined as the ratio of the actual turbine work per unit of total air flow (primary plus cooling) divided by the ideal work that would be achieved by expanding that total airflow through the actual pressure ratio.

$$\eta_t = \frac{(1-\varepsilon)(T_{04} - T_{05}) + \varepsilon(T_{0c} - T_{05})}{\left[(1-\varepsilon)T_{04} + \varepsilon T_{0c}\right]\left[1 - (p_{05}/p_{04})^{\gamma_t - 1/\gamma_t}\right]} \tag{3}$$

Here, T_{0c} is the stagnation temperature of the cooling air, T_{05} is the mean turbine exit temperature for the total flow, and ε [4] is the ratio of the cooling airflow to total airflow. Because cooling air is bled from the compressor, the power balance between the compressor and turbine is modified. Conservation of energy applied to the compressor includes the shaft power, P_S, provided to the compressor and the mass flow rate of the cooling air, $\dot{m}_c$.

The turbine energy balance is also modified by the addition of cooling air, the work done by the turbine, as well as the heat losses to the coolant [4].

$$(\dot{m} - \dot{m}_c - \dot{m}_f)c_{pt}T_{04} + \dot{m}_c c_{pc}T_{0e} = (\dot{m} - \dot{m}_f)c_{pt}T_{05} + P_S + Q \tag{4}$$

In this equation, T_{0e} is the stagnation temperature of the ejected coolant. In this equation, the heated coolant air is injected and mixed with the hot combustion product gases to the turbine exit temperature. The heat flux absorbed by the turbine blades, Q, is transferred to the coolant air to heat it from T_{0c} to T_{0e}.

Thus, for a given turbine inlet temperature, an optimal turbine cooling scheme is the one that keeps the maximum temperature in the metal blade at some limiting value with the lowest possible mass flow rate of the coolant.

To look at it from the viewpoint of the constraints, for a specified coolant mass flow rate, the turbine inlet temperature should be increased to the point where the maximum temperature of the blade material reaches its limit.

2. GEOMETRY PARAMETERIZATION

The size and shape of the mathematical space that contains all the design variables (for example, coordinates of all surface points) is very large and complex in a typical 3-D case. Only when it is possible to use simple and fast flow-field analysis codes could we afford an ideal optimization situation where each surface grid point on the 3-D optimized configuration is allowed to move independently. Otherwise, the designer is forced to somewhat restrict the design space by working with a relatively small number of the design variables by performing parameterization (fitting polynomials) of either the 3-D surface geometry or the 3-D surface pressure. The optimization code then needs to identify the coefficients in these polynomials. Since it is often necessary to constrain and sometimes not allow motion of certain parts of the 3-D surface, ***the most promising choices for the 3-D parameterization appear to be different***

types of Bezier [5] and local analytical [6,7]] surface patches for external and internal parameterize the 3-D blade geometry.

2.1. Geometry model of the turbine blade coating and internal coolant flow passages

The outer shape of the blade can be assumed as already defined by aerodynamic inverse shape design or optimization. It can be kept fixed during the entire thermal optimization procedure. The thermal barrier coating thickness could be described by a wall thickness function versus the airfoil contour-following coordinate, s. The material wall thickness variation around the blade could be defined by a piecewise-continuous beta-spline [5]. The number of coolant flow passages in the turbine blade is specified and kept fixed although a number of studies were published on inversely determining the number, sizes, shapes and locations of coolant flow passages [8-12].

The x-coordinates of the intersections of the centerlines of each of the internal struts with the outer turbine airfoil shape were defined as x_{Ssi} and x_{Spi}, for the suction and pressure sides of the blade, respectively. The range over which each strut could vary was specified. In addition to the coordinates of the strut intersections, the strut thickness, t_{Si}, and a filleting exponent on either the trailing or leading edge sides, e_{Sti} and e_{Sli}, respectively, were used to complete the geometric representation of each strut (Fig. 1a). The strut fillets were described by a super-elliptic function that varied from a circular fillet ($e_{Si} = 2$) to an almost sharp right angle ($e_{si} \to \infty$).

Total number of design variables per section of a three-dimensional blade was 27. These variables were: eight beta-spline control points defining coolant passage wall thickness, six strut end-coordinates (two per strut), three strut thicknesses (one per strut), six strut filleting exponents (two per strut), four relative wall roughnesses (one per each coolant flow passage). Two additional global variables were: one mass flow rate, and one inlet turbine hot gas temperature. The initial guess geometry is depicted in Figure 1b.

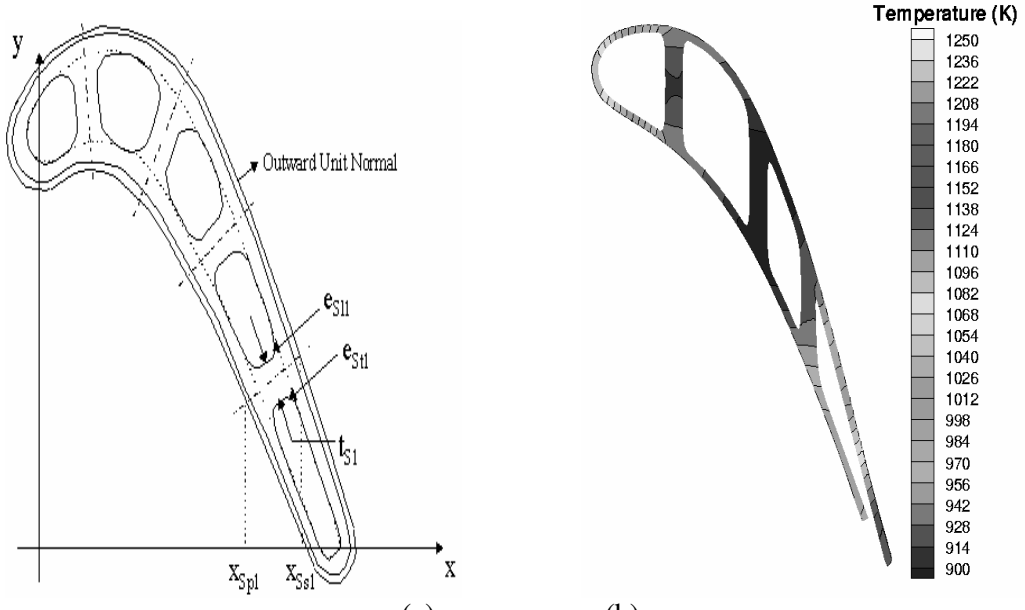

(a) (b)

Figure 1. (a) A sketch of turbine airfoil, coating and coolant passage parameterization; (b) Temperature field computed on the initial guess geometry used for the minimization of coolant temperature at the ejection location [13].

Another possibility is to parameterize the shapes of the internal coolant passages by using analytical shape functions [6,7]. The turbine blade considered in this example (Fig. 2) had a total of four straight passages connected by U-turn passages. The result is a single serpentine passage with a single inlet and outlet. The spanwise cross-sectional shape of each straight passage is described by four parameters (Fig. 2). These parameters (Fig. 3) include the filleting in the passage, r, the blade wall thickness, d, and the passage chordwise starting and finishing points, x_1 and x_2, respectively. The passage cross-section shapes are determined at the root and the tip by user provided parameter values. The parameters for the middle sections are found by linear interpolation along the blade span.

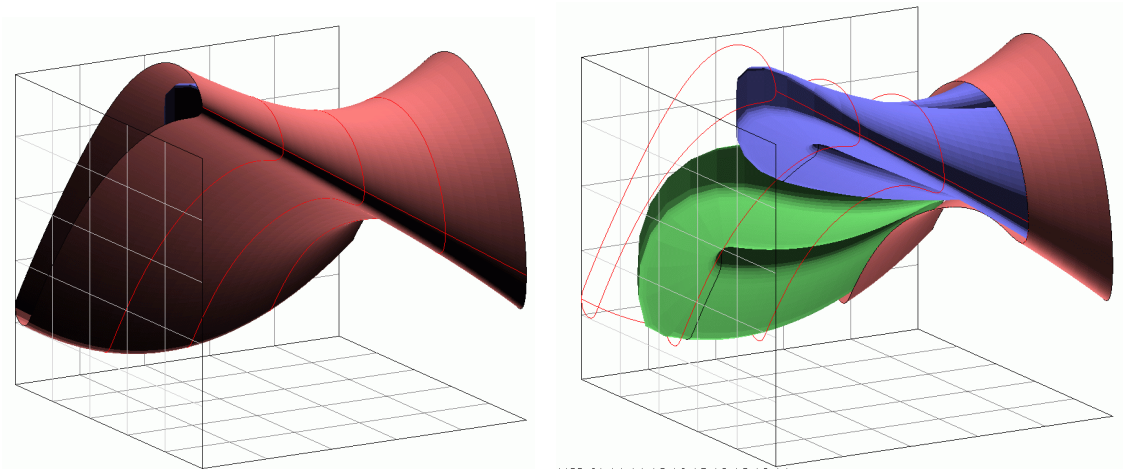

Figure 2: Generation of external and internal geometry of a 3-D cooled turbine blade using analytic surface patches formulation [7].

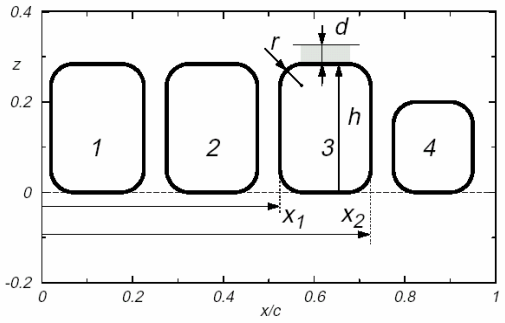

Figure 3: Parameters for passage cross-section shape in x-y plane

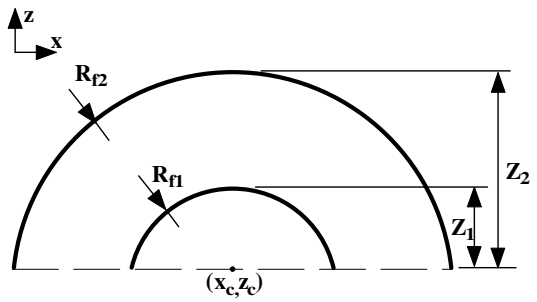

Figure 4: Parameters for U-turn shape in the x-z plane

Three U-turn shapes are used to connect the ends of the coolant passages (Fig. 4). The wall shape of the U-turn passage is determined by using analytic functions. Four parameters are needed to define each U-turn shape in the x-z plane as shown in Figure 4. The parameters Z_1 and Z_2 control the position of the passage walls in the z-direction. The parameters R_{f1} and R_{f2} control the roundedness of the U-turn shape. The following additional design parameters were also used: the coolant passage bulk temperature, T_c, and blade angle with the disk, θ_b. All together a total of 42 continuous design variables were used to uniquely describe a fully 3-D serpentine cooling passage configuration [14]. An equally smooth parameterization of the external configuration of the blade would require approximately 25-30 parameters. Notice that this approach to geometric discretization also guarantees the minimum allowable blade wall thickness anywhere.

3. Conjugate fluid flow/heat transfer analysis

The conjugate heat transfer problem is defined as the solution of the transport equations within the hot fluid flow coupled to the heat conduction equation within the solid blade region that is in contact with the fluid. Conjugate heat transfer analysis [15] typically involves an iterative coupling process between the two computational regions with separate analysis programs for the hot flow-field and for the blade material heat conduction [16,17]. Thermal stress analysis in the blade is typically carried out afterwards.

3.1. An iterative conjugate analysis approach

An efficient preliminary design optimization of 3-D coolant flow passage could be a combination of: a) a detailed analytical model and computations of the sectional 2-D hot gas flow-field, b) an accurate 3-D boundary element heat conduction analysis code in the blade material, and c) the presently available experimentally obtained correlations comprising a metamodel for the heat transfer from the blade to the coolant [12,13].

First, a turbulent compressible flow Navier-Stokes solver was used to predict the hot gas flow-field outside of the blade subject to specified realistic hot surface temperature distribution. As a byproduct, this flow-field analysis provides hot surface normal temperature gradients thus defining the hot surface convection heat transfer coefficient distribution. This and the guessed coolant bulk temperature and the coolant passage wall convection heat transfer coefficients creates boundary conditions for the steady temperature field prediction in the blade and thermal barrier coating materials using a fast boundary element technique. The quasi 1-D flow analysis (with heat addition and friction) of the coolant fluid dynamics is then coupled to the detailed steady heat conduction analysis in the turbine blade material. By perturbing the design variables (especially the variables defining the internal blade geometry) the predicted thermal boundary conditions on the interior of the blade will be changing together with the coolant flow parameters. As the optimization algorithm ran, it also modified the turbine inlet temperature. Once the turbine inlet temperature changed significantly, the entire iterative procedure between the thermal field analysis in the blade material and the computational fluid dynamic analysis of the external hot gas flow-field needs to be performed again to find a better estimate for thermal boundary conditions on the blade hot surface. This global coupling process needs to be performed only a small number of times during the course of the entire optimization. This solution strategy required only 9-12 hot gas flow-field solutions [12,13,18].

Thus, this quasi 3-D conjugate analysis uses sectional two-dimensional blade hot flow-field analysis, a separate heat conduction analysis code for the blade material structure, and a simple quasi one-dimensional coolant flow-field analysis. Consequently, it requires considerably less computing time than would be needed if a full 3-D hot gas flow-field and coolant flow-field analysis [19] would be used.

3.2. Fully coupled 3-D conjugate fluid flow/heat transfer analysis

Recently, 2-D and a fully 3-D conjugate heat transfer prediction code was developed [20] where the compressible turbulent flow Navier-Stokes equations analysis code is used simultaneously in the flow-field and in the solid material of the blade structure thus automatically predicting correct magnitudes and distribution of surface temperatures and heat fluxes. The only thermal boundary conditions are the convection heat transfer coefficients specified on the surfaces of the internal coolant flow passages. This approach eliminates the need to specify hot surface temperature or heat flux distribution. The CFD code uses non-

structured triangular grids in 2-D and tetrahedral grids in 3-D in the flow-field and in the blade structure (Fig. 5). The code has been successfully tested on internally cooled turbine airfoil cascades and on fully 3-D stator blades (Fig. 6). The conjugate solution of the 3-D hot gas flow-field and the temperature field inside the 3-D blade structure consumes only about 20-25 percent more computing time than the typical CFD solution of the 3-D hot flow-field alone.

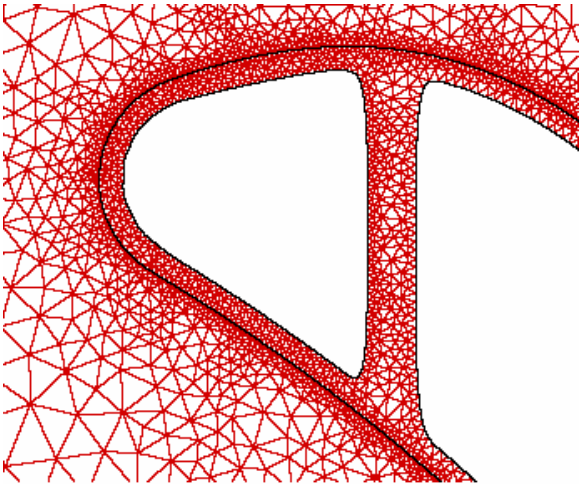

Figure 5: A non-structured computational grid for conjugate heat transfer analysis [20].

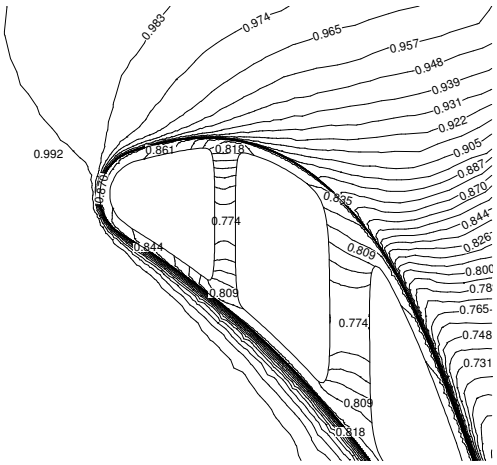

Figure 6: Isotherms predicted using a conjugate analysis of a 3-D blade [20].

3.3. Thermal-elasticity analysis

Our current linear thermo-elasticity analysis code [66] uses a finite element method (FEM) on a tetrahedral non-structured grid, ILU and multilevel preconditioned Krylov subspace methods, object-oriented programming in C++, and symbolically integrated linear and quadratic elements [21]. The code can run on any standard Windows NT or Unix platform. The FEM code takes only half a minute on a personal computer with a 3.0 GHz Pentium processor to compute detailed steady stress and deformation fields in a single material 3-D internally cooled gas turbine blade with three coolant flow passages and 150,000 degrees of freedom.

3.4. Computational grid effects

It is well-known that computational grid features (clustering, orthogonality, cell aspect ratios, grid refinement, etc.) could affect iterative convergence rate of a computational flow analysis algorithm and also the level of accuracy of the numerical results. The following several figures illustrate the seriousness of these issues when using non-structured triangular cell grids (Figs. 7 and 8) and hybrid grids (Fig. 9) consisting of several layers of quadrilateral cells next to a solid boundary and triangular cells in the rest of the field. For example, the difference between grid10 and grid11 is the distance between the first O-grid layer and the surface of the blade. For the grid10 such distance is equal to 0.001 mm and for the grid11 the distance is equal to 0.1 mm. Consequently, any numerical analysis computer code intended for use in the multi-disciplinary design optimization should be thoroughly tested for its accuracy on a variety of computational grids prior to applying it in actual design optimization.

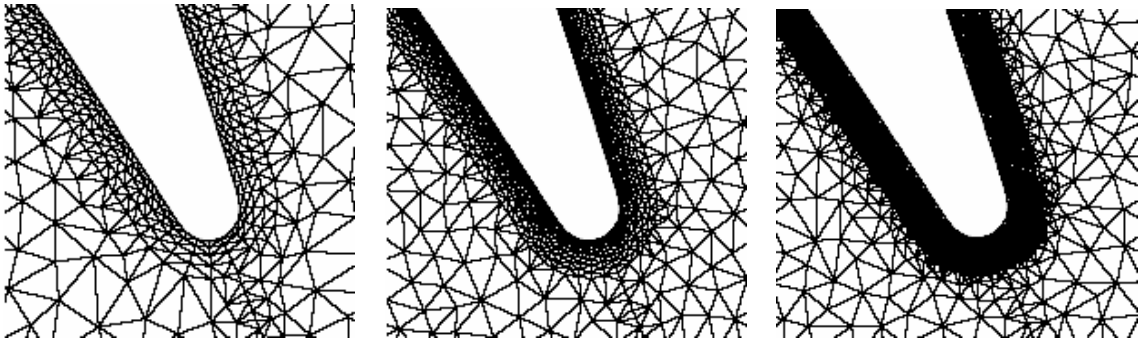

Figure 7: Computational grids number 2, 4 and 5 producing CFD results depicted in Fig.8.

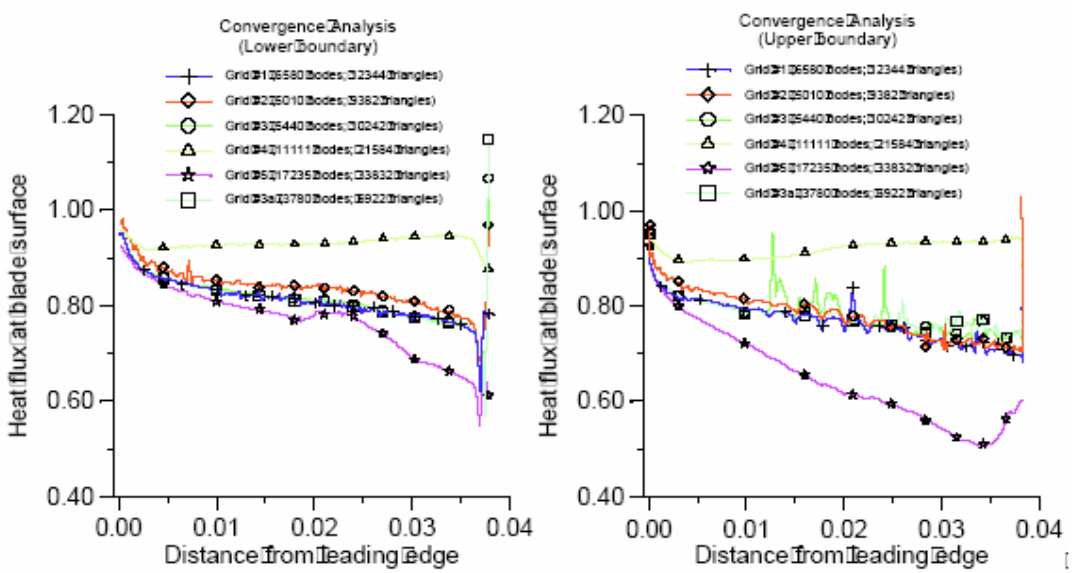

Figure 8: CFD results using turbulent Navier-Stokes equation solver on various grids.

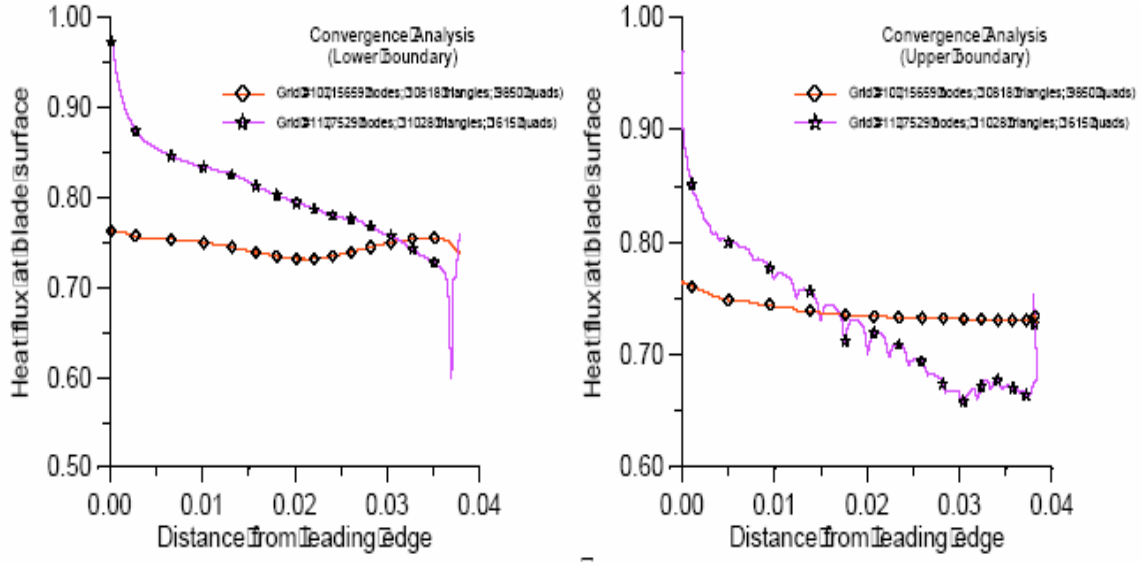

Figure 9: Transonic cascade turbulent flow results using a NSE solver on various hybrid grids.

3.5. Fast analysis of multi-stage axial gas turbine performance at design and off-design

The application of fully 3-D methods for analysis of realistic multi-stage turbomachinery flows meets several serious challenges. The handling of consecutive blade rows with relative movement entails either averaging procedures or unsteady time-accurate flow calculations. Furthermore, the validity of turbulence models for loss calculation commonly used in the fully 3-D methods is still questionable. Influence of numerical dissipation and correct formulations of non-reflecting boundary conditions are still not fully resolved issues in these types of calculations. Reliability of the full 3-D multi-stage flow-field analysis using a complete Navier-Stokes system is still questionable especially at off-design operating conditions. But, most importantly, using a fully 3-D multi-stage Navier-Stokes analysis code as a module in a design optimization process is unacceptable since it poses exorbitant requirements on computing time and computer memory. Therefore, a significant interest exists especially in industry to further improve fast through-flow analysis methods combined with empirical loss coefficients as a first step in the design of multi-stage machines. The general through-flow analysis model represents a simplified model (a surrogate) compared to a fully 3-D unsteady Navier-Stokes system of non-linear partial differential equations governing multi-stage turbomachinery aerodynamics. In recent works by M. V. Petrovic, [22,23], the well-known through-flow analysis theory was augmented with new combinations of loss and deviation correlations and with an extension to encompass reverse flow in meridional plane.

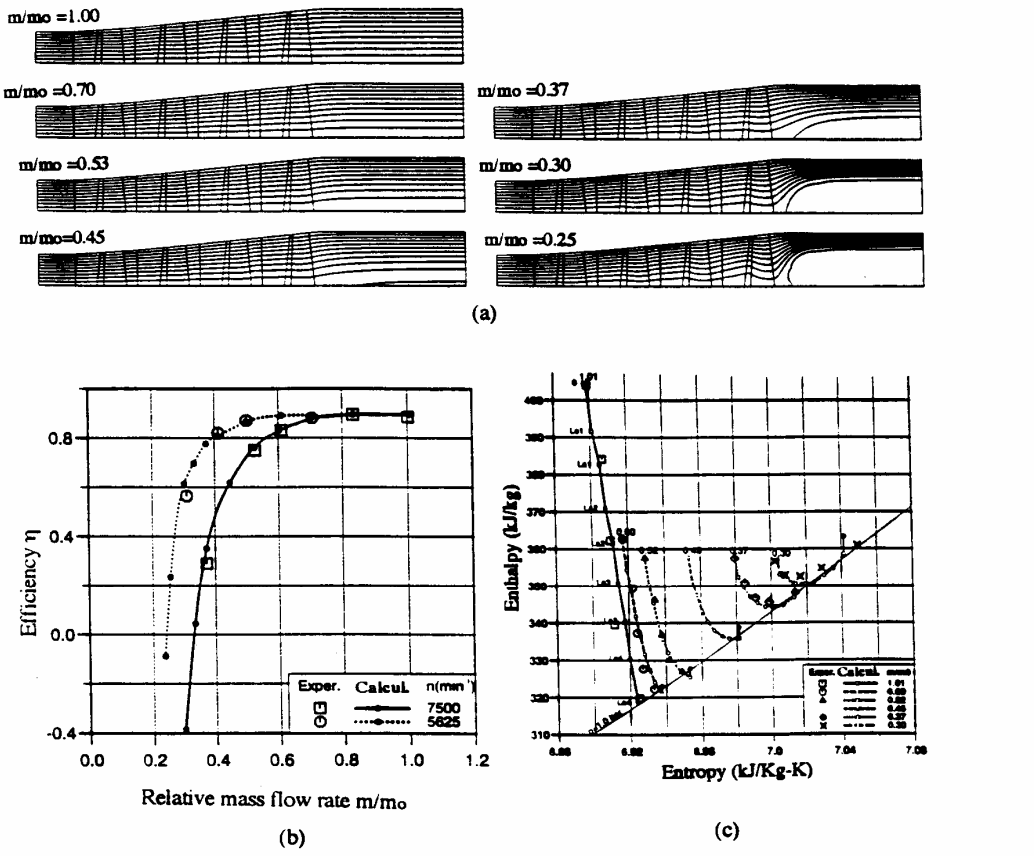

Figure 10: The through-flow analysis shows excellent agreement with experimental data for a four-stage uncooled axial turbine over a range of relative mass flow rates. (a) streamlines correctly predicting flow separation, (b) aerodynamic efficiency at two different rotational speeds, and (c) comparison with experiments for enthalpy-entropy performance map [22,23].

Petrovic's models for the loss coefficient prediction, the spanwise loss distribution, the spanwise mixing, and spanwise deviation distribution, resulted in calculations that are in excellent agreement with experimental data for overall multi-stage turbine efficiency at full and partial fluid mass flow rates (Fig. 10). Prof. Petrovic found that the conventional through-flow methods supply wide range performance data of good quality and even correctly predict the local flow reversal without any modeling effort involving fully 3-D flow calculations. This through-flow analysis code applied to a four-stage turbine takes approximately three minutes on a standard 3.0 GHz processor to predict an operating map that consists of ten different operating conditions.

4. Optimization algorithms

A number of existing and emerging concepts and methodologies applicable to automatic inverse design and design optimization of arbitrary realistic 3-D configurations have been surveyed and compared [24-26], with the following conclusions:

- *Most of the existing 3-D shape inverse design methods are based on inviscid fluid models, assume small geometry changes, and require significant changes to the flow analysis codes,*
- *Gradient search sensitivity-based optimization methods are very computationally intensive and unreliable for large shape optimization problems since they terminate in the nearest available local minima thus offering only minor design improvements,*
- *Brute force application of genetic evolution optimizers is very computationally intensive for realistic 3-D shape optimization problems that involve a number of equality constraints, and*
- *Adjoint operator (control theory) algorithms are too field-specific and governing equation specific, complex to understand and develop, hard to modify, and prone to local minima.*

4.1. Our original hybrid optimizer

A hybrid optimization method that we developed in the 90's [27] has the following optimization modules; the Davidon-Fletcher-Powell (DFP) Gradient method [28,29], a Genetic Algorithm (GA) [30], the Nelder-Mead (NM) Simplex method [31], quasi-Newton algorithm of Pshenichny-Danilin (LM) [32], Differential Evolution (DE) [33], and Sequential Quadratic Programming (SQP) [34].

Each of these basic optimization algorithms provides a unique approach to optimization with varying degrees of convergence, reliability and robustness at different cycles during the iterative optimization procedure. A set of analytically formulated rules and switching criterion were coded into the program to automatically switch back and forth among the different optimization algorithms as the iterative minimization process proceeded [27]. The hybrid algorithm handles the existence of equality and inequality constraint functions in three ways: Rosen's projection method, feasible searching, and random design generation. Rosen's projection method provided search directions that guided descent-directions tangent to active constraint boundaries. In the feasible search, designs that violated constraints were automatically restored to feasibility via the minimization of the active global constraint functions. If at any time this constraint minimization failed, random designs were generated about the current design until a new feasible design was reached. Gradients of the objective and constraint functions with respect to the design variables, also called design sensitivities, were calculated using either finite differencing formulas, or by a more efficient method of implicit differentiation of the governing equations [35]. The population matrix was updated every iteration with new designs and ranked according to the value of the objective function.

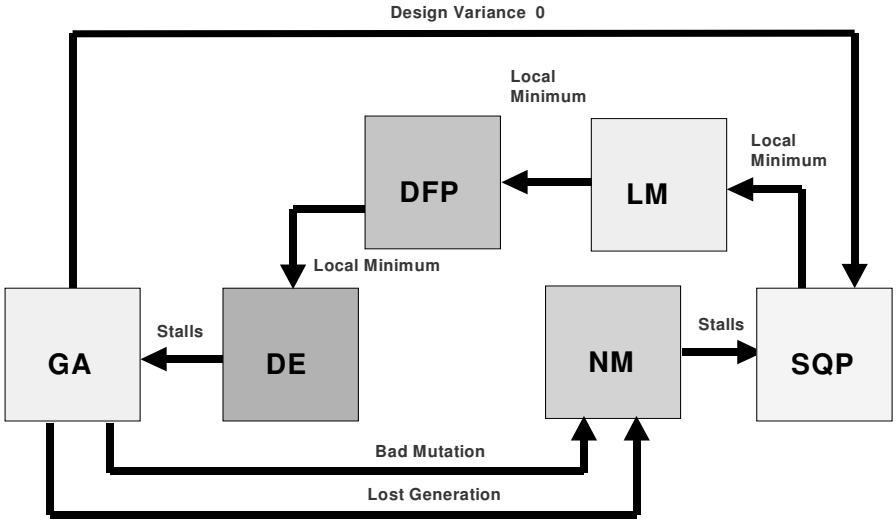

Figure 11: Global procedure for the older version of our old hybrid optimization method [27].

During the optimization process, local minimums can occur and halt the process before achieving an optimal solution. In order to overcome such a situation, a simple technique has been devised for switching objective function formulations [8-10]. Whenever the optimization stalls, the formulation of the objective function is automatically switched between two or more forms that can have a similar purpose (Fig. 11). The optimization problem was completed when the maximum number of iterations or objective function evaluations were exceeded, or when the optimization program tried all individual optimization algorithms but failed to produce a non-negligible decrease in the objective function. The latter criterion was the primary qualification of convergence and it usually indicated that a global minimum had been found. This hybrid optimization method was successfully applied to problems involving the estimation of the diffusion coefficient and source terms [36] as well as problems involving magnetohydrodynamics [37,38] and electrohydrodynamics [39].

4.2. Our recent hybrid optimizer

Our most recent hybrid optimization method [40] is quite simple conceptually, although its computational implementation is more involved. The global procedure is illustrated in Figure 12. The driven module is very often the Particle Swarm method [41], which often performs most of the optimization task. When certain percent of the particles find a minima (let us say, some birds already found their best nesting place), the algorithm switches automatically to the Differential Evolution method [33] and the particles (birds) are forced to breed. If there is an improvement in the objective function, the algorithm returns to the Particle Swarm method, meaning that some other region is more likely to having a global minimum. If there is no improvement on the objective function, this can indicate that this region already contains the global value expected and the algorithm automatically switches to the BFGS method [41] in order to find its location more precisely. In Figure 12, the algorithm returns to the Particle Swarm method in order to check if there are no changes in this location and the entire procedure repeats itself. After some maximum number of iterations is performed (e.g., five) the process stops. In the Particle Swarm method, the probability test of the Simulated Annealing is performed in order to allow the particles (birds) to escape from local minima, although this procedure most often does not make any noticeable improvement in the method. Notice that this hybrid optimization method differs considerably from the earlier version that performed automatic switching among six classical optimization modules.

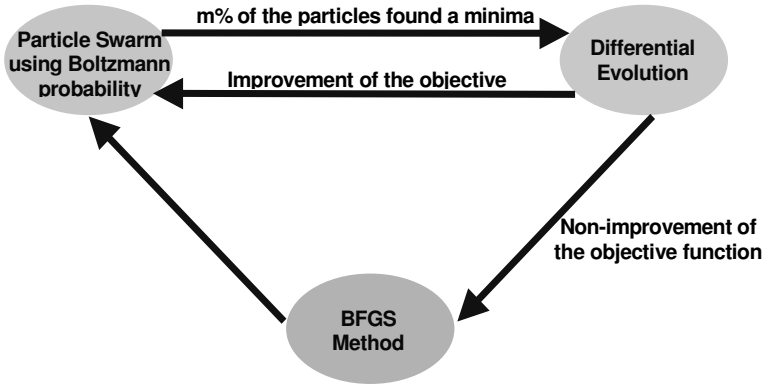

Figure 12: Global procedure for our new hybrid optimization method [42].

As a demonstration of the superior performance of a hybrid optimizer when compared to individual optimization algorithms, we will show the performance of several of the optimizers to find the optimum of the Griewank's function [43], which is defined as

$$U = \sum_{i=1}^{n} \frac{x_i^2}{4000} - \prod_{i=1}^{n} \cos\left(\frac{x_i}{\sqrt{i}}\right) + 1 \qquad (5)$$

$$x \in]-600,600[$$

The global minima for this function is located at $\mathbf{x} = 0$ and is $U(\mathbf{x}) = 0$. For a two-dimensional test case, such function is shown in Figure 13 in three levels of local resolution. One can see that this function has an extremely large number of local minima, making the optimization task of finding the global minimum quite a challenge.

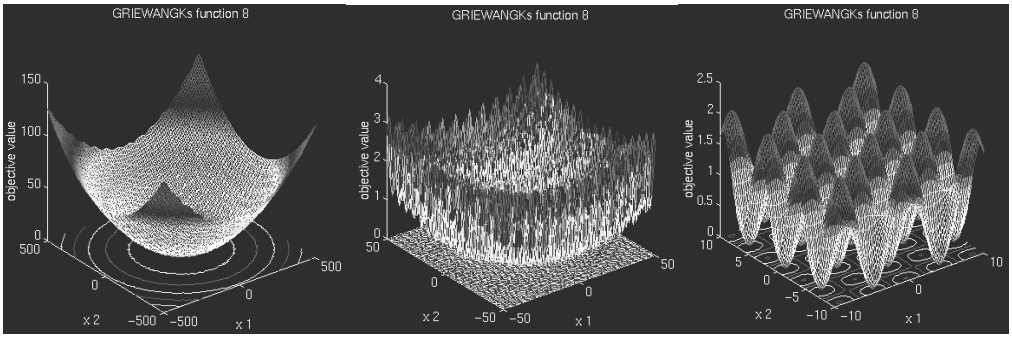

Figure 13: Griewank's function: global view, intermediate view, local view.

Figure 14 shows the results [42] for this optimization task using the (a) BFGS, (b) differential evolution, (c) simulated annealing, (d) particle swarm and (e) our new hybrid optimization methods. One can see that the evolutionary/stochastic methods are a little bit better than the BFGS method. However, only the new hybrid optimization method is capable of locating the global optimum value of this function.

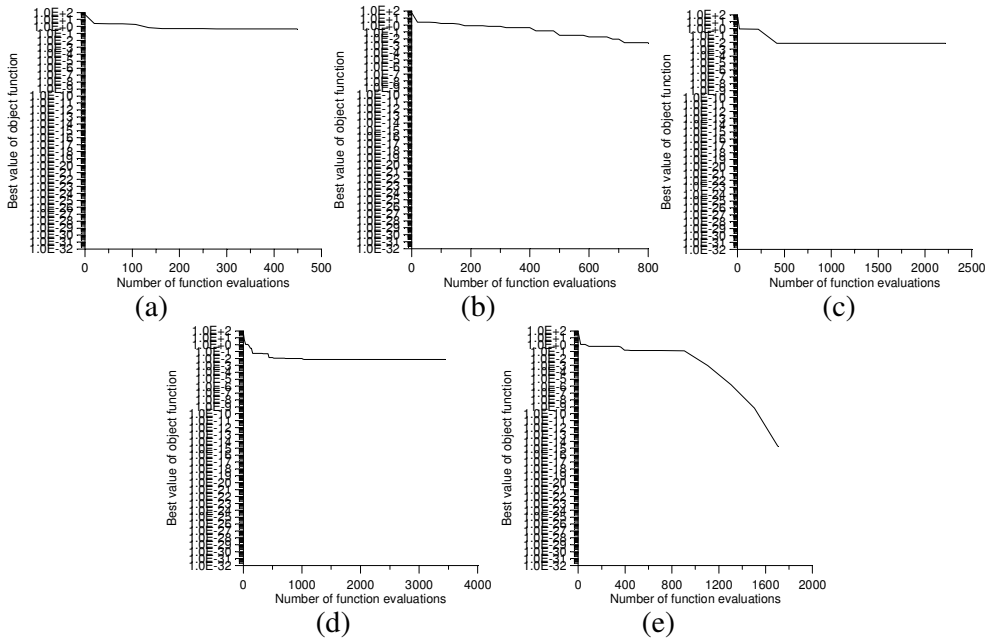

Figure 14: Comparison of the optimizers for the Griewank's function [42].

4.3. Method of Indirect Optimization based upon Self-Organization (IOSO) and evolutionary simulation principles [44-50]

The IOSO method is a constrained optimization algorithm based on self-adapting response surface methods and evolutionary simulation principles. Each iteration of IOSO consists of two steps. The first step is the creation of a local approximation of the objective functions. Each iteration in this step represents a decomposition of an initial approximation function into a set of simple approximation functions (Fig. 15). The final response function is a multi-level graph (Fig. 16). The second step is the optimization of this approximation function. This approach allows for self-corrections of the structure and the parameters of the response surface approximation to make it more accurate in regions of the design space that promise rapid convergence.

The obtained response functions are used in the procedures of multi-level optimization with the adaptive changing of the simulation level within the frameworks of both single and multiple disciplines of the object analysis. During each iteration of IOSO, the optimization of the response function is performed only within the current search area. This step is followed by a direct call to the mathematical analysis model for the obtained point. During the IOSO operation, the information concerning the behavior of the objective function in the vicinity of the extremum is stored, and the response function is made more accurate only for this search area. Thus, a series of approximation functions for a particular objective of optimization is built at each iteration. These functions differ from each other according to both structure and definition range. The subsequent optimization of these approximation functions allows us to determine a set of vectors of optimized variables, which are used for the computation of optimization objectives on a parallel computer.

For a basic parallel IOSO algorithm, the following steps are carried out:

1. Generate a group of designs based on a design of experiments (DOE) method;
2. Evaluate the designs in parallel with the analysis code;
3. Build initial approximation based on the group of evaluated designs;
4. Use stochastic optimization method to find the minimum of the approximation;
5. Do adaptive selection of current extremum search area;

6. Generate a new set of designs in current extremum search area using DOE;
7. Evaluate the new set of designs in parallel with the analysis code;
8. Update the approximation with newly obtained result;
9. Goto 4, unless termination criteria is met.

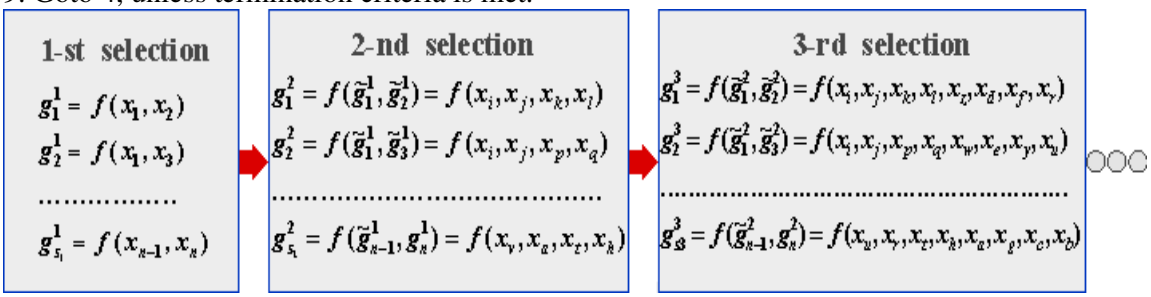

Figure 15: A decomposition of an initial approximation function into a set of simple approximation functions.

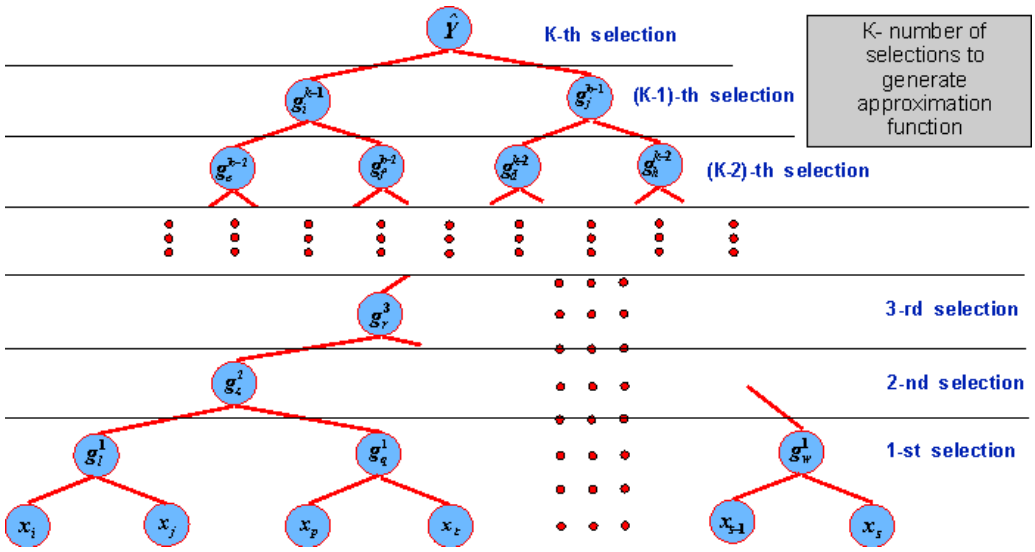

Figure 16: The final response function is a multi-level graph

The distinctive feature of IOSO algorithm is an extremely low number of trial points to initialize the algorithm (30-50 points for the optimization problems with nearly 100 design variables). In addition, IOSO was successfully applied to problems with hundreds of design variables and a large number of constraints and objective functions.

If a large number of processors are available, the optimizer can use all of them by running several simultaneous parallel analyses to evaluate several candidate design configurations. For this research an optimization communication module was developed using the MPI library [47] that utilizes this multi-level hierarchy of parallelism. This module can be used with any parallel optimization method including GA and IOSO algorithms.

Multi-objective optimization algorithms [46] have been successfully applied in a number of engineering disciplines. Such algorithms are needed to solve actual multi-disciplinary industrial application design problems having hundreds of highly constrained design variables and several simultaneous objectives. However, for a rapidly increasing number of mixed real and integer design variables, constraints, and objectives that need to be extremized simultaneously, these algorithms become too time consuming for practical applications in industry.

In multi-objective optimization we strive to compute the group of the *not-dominated* solutions, which is known as the Pareto optimal set, or Pareto front. These are the feasible solutions found during the optimization that cannot be improved for any one objective without degrading another objective. We have found that the multi-objective constrained optimization algorithm that is superior to any other currently available multi-objective optimizers is IOSO. The effectiveness of IOSO optimization procedure has been demonstrated with the examples of car engine exhaust toxicity minimization (3 variables, 4 objectives) [48], optimal control laws for the power plant of a short take-off and vertical landing aircraft for its take-off mode (50 variables, 2 objectives) [49], the preliminary solution of the problem of a multi-stage axial compressor optimization aimed at its efficiency maximization (42 variables, 2 objectives) [50], and optimization of concentration of alloying element in a minimum expensive superalloy for maximum strength, time-to-rupture, and temperature (14 variables, 10 objectives) [51].

5. Examples of design optimization results

The typical situation when solving real life multi-objective Multi-Disciplinary Optimization (MDO) problems [46] is that a designer has several tools available for performing the analysis. These analysis tools differ according to their levels of complexity and accuracy. The low-fidelity analysis models allow us to carry out optimization, but the validity of the obtained results can be rather low because of the simplified physical model. The high-fidelity analysis tools can be the detailed non-linear mathematical models integrated on the finest computational grid possible or even the experimental samples of the system or its components. However, the exclusive use of such high-fidelity tools in multi-objective MDO is associated with significant time expenditures and is therefore unacceptable for practical use.

5.1. Preliminary aerodynamic optimization of a multi-stage axial gas turbine

We have recently developed and published [52,53] a system for preliminary design optimization of geometric and flow-field parameters of multi-stage transonic axial flow turbines at nominal and off-design conditions. An analysis of the loss correlations was made to determine which parameters have the most profound influence on the turbine performance. It was found that by varying at least seventeen variables (eight geometric and nine flow-field parameters) per each turbine stage, it is possible to evaluate an optimal radial distribution of flow parameters at inlet and outlet of each blade row and an optimal shape of hub and shroud. The optimized solution gives the maximum efficiency of the multi-stage axial turbine and is, at the same time, technically acceptable. The design system has been demonstrated on an example (Fig. 17) involving a well-documented set of experimental data for a one-stage uncooled transonic axial gas turbine [54]. The comparison of computed performance of initial and optimized designs shows significant improvement in the optimized multi-stage efficiency (Fig. 18). It is easy to see that this exceptionally fast preliminary design optimization system reduces entropy generation in multi-stage turbomachinery (Fig. 19 and Fig. 20). The entire design optimization process was found to be computationally quite feasible consuming 0.75 hours on a single processor SGI R10000 workstation. Such extraordinary speed of execution was possible mainly because of the use of a highly accurate through-flow metamodel instead of the complete Navier-Stokes 3-D rotor-stator unsteady compressible turbulent flow-field analysis code.

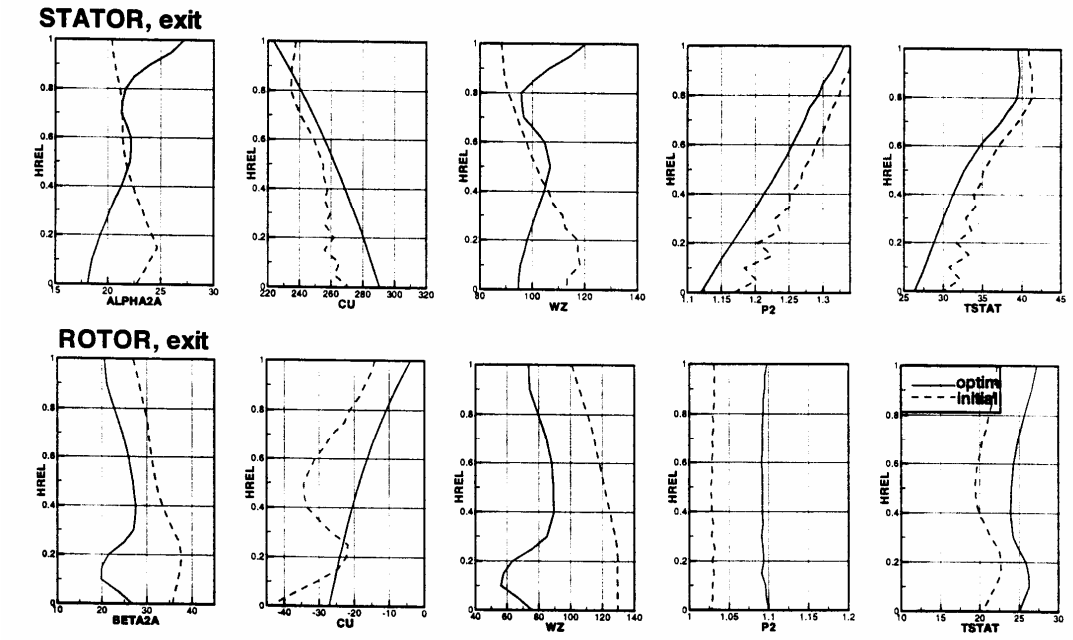

Figure 17. Initial values (dashed line) and optimized values (full line) of radial distributions of: ALPHA2 (exit flow angle, absolute flow – degrees), BETA2 (exit flow angle, relative flow – degrees), CU (tangential component of absolute velocity – m/s), WZ (axial velocity – m/s), P2 (static pressure – bar), T2 (static temperature – C). The configuration was a single stage transonic uncooled axial gas turbine [52].

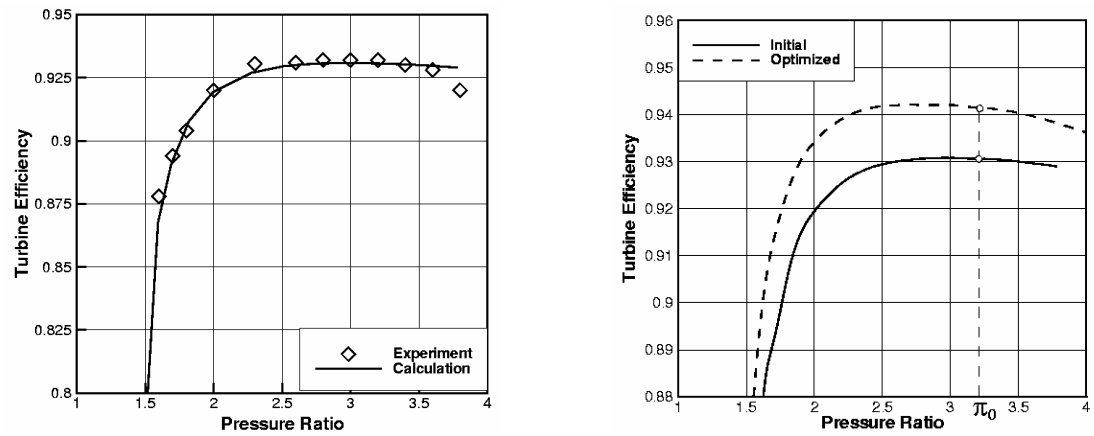

Figure 18: Turbine efficiency over a range of pressure ratios: a) comparison of experimental data (symbols) and analysis using an axisymmetric flow analysis with losses model, b) comparison with results obtained after performing optimization with a hybrid optimizer [51].

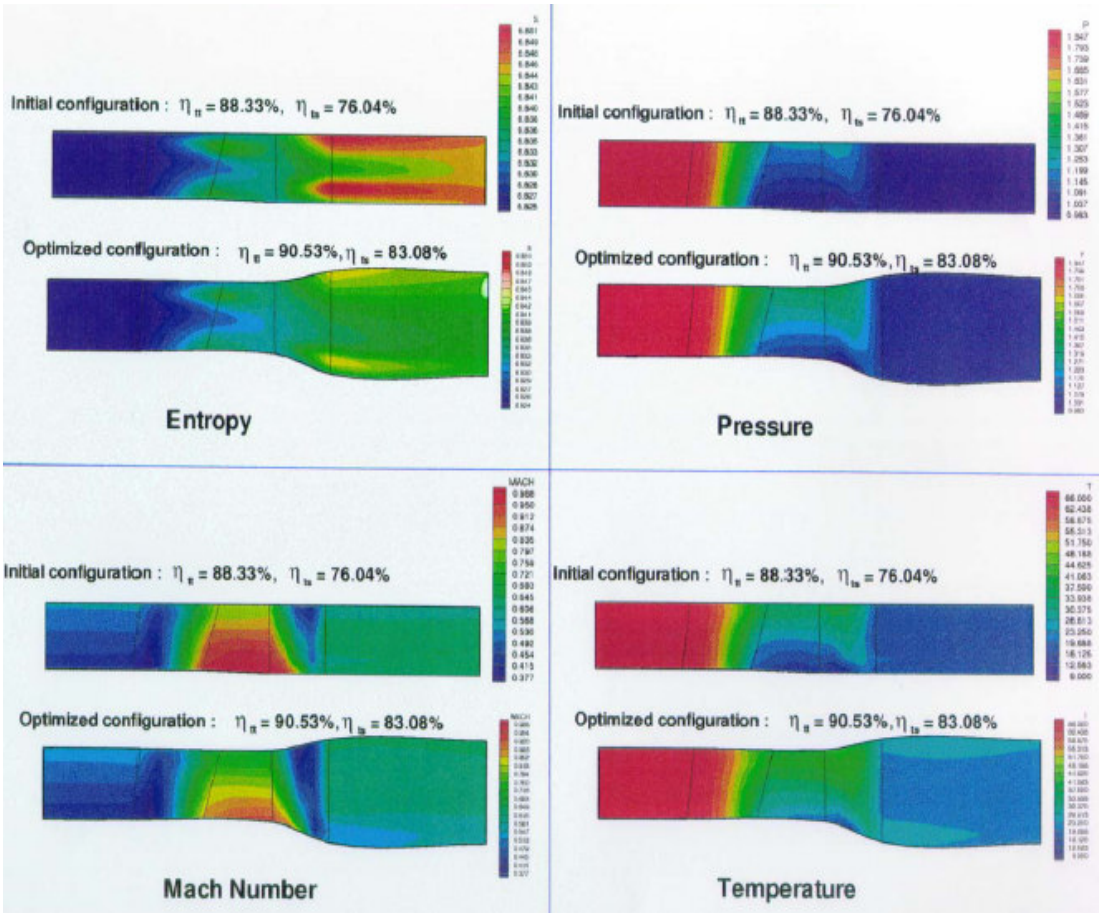

Figure 19: Fields of entropy, Mach number, pressure and temperature before and after the optimization of the hub and shroud shapes using the original version of hybrid optimizer.

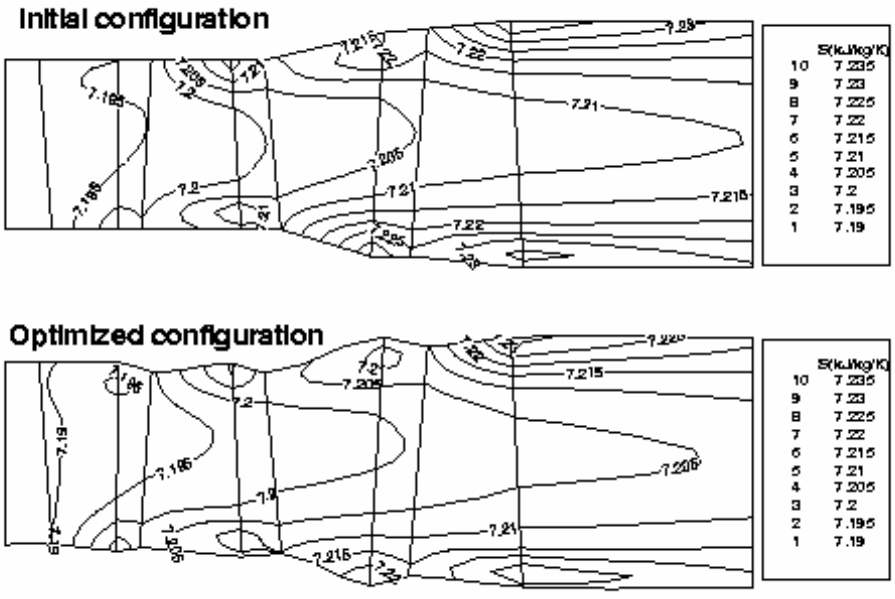

Figure 20: Constant entropy curves in the original and the optimized configuration of a two-stage axial gas turbine demonstrate – results of using axisymmetric flow analysis with losses and our original version of hybrid optimization while varying hub and shroud shapes [53].

5.2. Preliminary design optimization of 3-D blade dihedral and sweep angles variations

We have recently performed an attempt at optimizing some aspects of an actual 3-D transonic stator blade. The objective was to determine radial distribution of sweep and dihedral angles of an axial turbine stator blade with given sectional airfoil shapes and a given twist so that the integrated total pressure loss is minimized. This was achieved while satisfying a number of constraints, e.g., fixed axial chord, inlet and exit flow angles, inlet total pressure and temperature, exit average static pressure, and mass flow rate. The radial variation of these two angles was parameterized using Bezier curves with four control points in terms of the radial coordinate. The optimization procedure then determined the proper values of the coefficients in these curves that gave the most efficient 3-D blade shape. Because of the significant variation of the 3-D blade shapes during the optimization process, the analysis of the performance of intermediate 3-D blade shapes was evaluated using our unstructured grid compressible Navier-Stokes CFD code with k-ε turbulence model. An analysis of the flow-fields of the initial and the final blade shapes reveals that strengths of the secondary flows have been decreased due to the optimized sweep and dihedral distributions. The result is a decrease of the entropy at the exit plane and decrease of 3% in the overall loss coefficients.

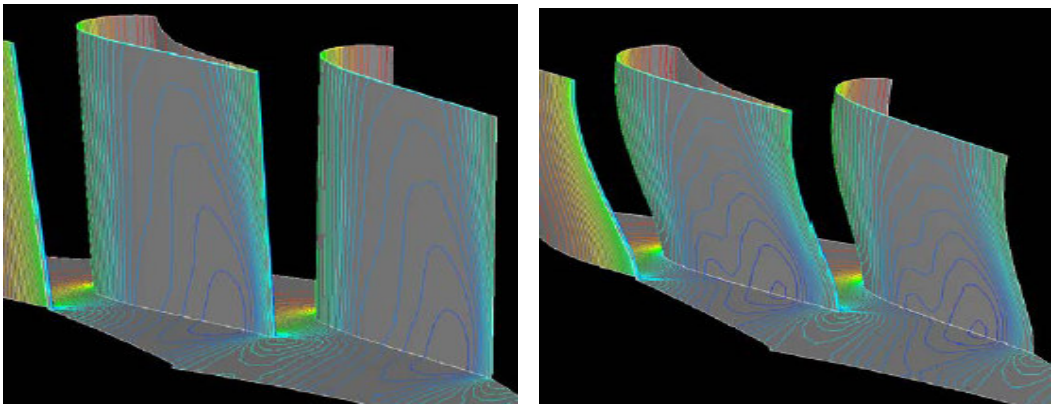

Figure 21: Initial configuration of 3-D stator blades (left) and final configuration (right) after performing optimization of radial variations of sweep and dihedral angles.

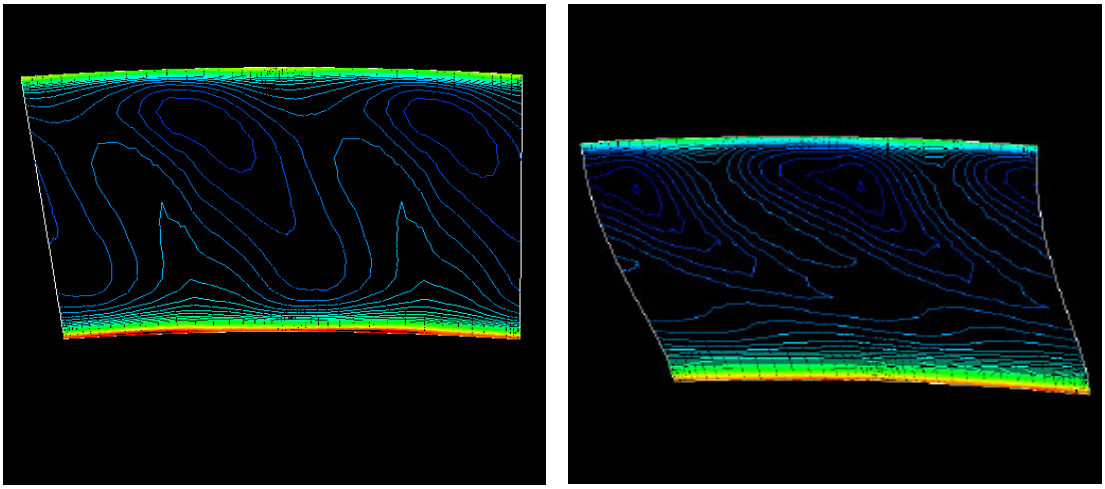

Figure 22: Initial distribution of constant entropy levels at the exit plane (left) and final distribution (right) after optimization of radial variations of sweep and dihedral angles.

6. Multi-objective optimization of airfoil cascades for minimum loss, maximum loading, and maximum gap-to-chord ratio [55]

This work illustrates an automatic multi-objective design optimization of a two-dimensional airfoil cascade row having a finite number of airfoils. The objectives were to simultaneously minimize the total pressure loss, maximize total aerodynamic loading (force tangent to the cascade), and minimize the number of airfoils in the finite cascade row [55]. The constraints were: fixed mass flow rate, fixed axial chord, fixed inlet and exit flow angles, fixed blade cross-section area, minimum allowable thickness distribution, minimum allowable lift force, and a minimum allowable trailing edge radius. This means that the entire airfoil cascade shape was optimized including its stagger angle, thickness, curvature, and solidity. The analysis of the performance of intermediate airfoil cascade shapes were performed using our unstructured grid based Navier-Stokes compressible flow-field analysis code with k-ε turbulence model.

The *multi*-objective constrained optimization algorithm used in this work is the modified version of an indirect method of optimization based upon self-organization (IOSO). The airfoil shape was defined with the following nine parameters: the tangential and axial chord, the inlet and exit half wedge angle, the inlet and outlet airfoil angle, the throat, unguided turning angle, and the leading and trailing edge radii [56]. One of these parameters (axial chord) was kept fixed. The airfoil shape was allowed significant additional flexibility by adding a continuous arbitrary perturbation in addition to the original nine parameters. This shape perturbation was modeled with a B-spline that had eight control vertices thus resulting in a total of 9 + 8 = 17 design variables plus one additional variable for the number of airfoils in a finite length cascade. Thus, there were 18 design variables in this case. The design variables' ranges were set so that the optimizer would have a wide variety of very different airfoil shapes so as to test its robustness. With these conditions we defined the following 3 objectives (Table 1) and the 5 nonlinear constraints (Table 2) for a VKI high subsonic exit flow axial turbine cascade [57].

Table 1. Simultaneous objectives in the multi-objective constrained optimization

	OBJECTIVES
MAXIMIZE	Total loading force
MINIMIZE	Total pressure loss
MINIMIZE	Number of airfoils

Table 2. Inequality and equality constraints used

CONSTRAINTS	Values
Total loading	> 186599 N
Mass flow rate (per unit span)	= 384 kg m^{-1} s^{-1}
Exit flow angle	= -70°
Airfoil cross-section area	= 108.8 mm^2
Airfoil trailing edge radius	= 0.5 mm

The constraints were incorporated in the objective functions via penalty formulation.

$$F_1 = p_o^{outlet} - p_o^{inlet} + c_1\left(\frac{-70.0-\theta}{-70.0}\right)^2 + c_2\left(\frac{384.0-\dot{m}}{384.0}\right)^2 + c_3\left(\frac{0.0001088-A}{0.0001088}\right)^2 + c_4\left(\frac{186599-L}{L}\right)^2 + c_5(td)^2 \quad (6)$$

$$F_2 = -L + c_1\left(\frac{-70.0-\theta}{-70.0}\right)^2 + c_2\left(\frac{384.0-\dot{m}}{384.0}\right)^2 + c_3\left(\frac{0.0001088-A}{0.0001088}\right)^2 + c_4\left(\frac{186599-L}{L}\right)^2 + c_5(td)^2 \quad (7)$$

$$F_3 = nb \quad (8)$$

Here, p_0 is the total pressure, θ is the average exit flow angle, $\dot{m}$ is the mass flow rate, A is the cross-sectional area of the airfoil, *nb* is the total number of airfoils, and L is the total loading. The variable *td* is the largest relative error in the airfoil thickness distribution compared to a specified minimum allowable thickness distribution. This geometric constraint prevents airfoil from becoming too thin, thus mechanically or thermally infeasible. The constants c_i are user specified penalty terms. For this application, the penalty constants were initially set to 100000. A value of zero was used for the constants when any of the constraints were within one percent above or below the target constraint value.

Table 3. A comparison of the three objectives achieved by the original VKI cascade and the three prominent cascades obtained with our multi-objective constrained optimization.

	VKI	No.1	No.3	No.6
Total pressure loss, Pa	103078	95164	97050	95012
Total loading, N	186599	189359	196778	193228
Number of airfoils	45	44	46	45

The resulting hint of a Pareto front is depicted in Fig. 23 and shapes of the resulting airfoils are shown in Fig. 24.

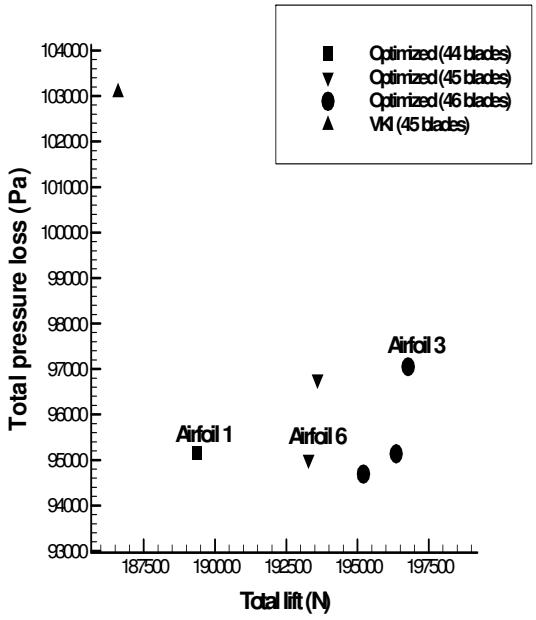

Figure 23: Comparison of total pressure loss generated versus total loading produced for various numbers of airfoils for optimized airfoil cascades and the VKI airfoil cascade.

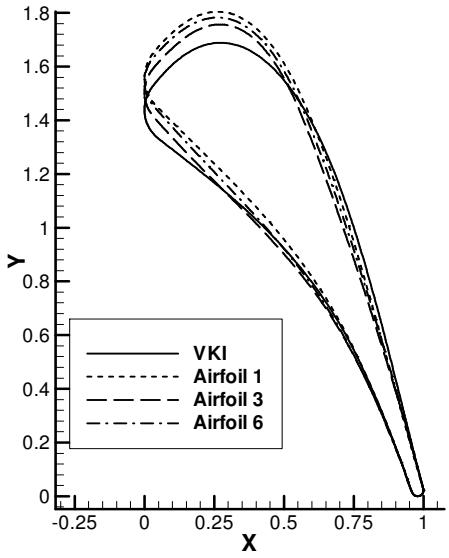

Figure 24: Comparison of three optimized airfoil cascades [55] against the original VKI airfoil cascade [57].

Cascade No.1 offers reduction of 7% in total pressure loss, needs 1 airfoil less than the VKI cascade, and generates about 1% higher total loading. Cascade No.3 offers reduction of 5% in total pressure loss, need 1 more airfoil than the VKI cascade, and generates about 6% higher total loading. Cascade No.6 offers reduction of 7% in total pressure loss, need the same number of airfoils as the VKI cascade, and generates about 4% higher total loading. The cascade No.1 may be the best compromise among three optimized cascades for many turbomachinary designs.

This means that it is possible to design turbomachinery blade rows that will have simultaneously lower total pressure loss, higher total loading, and fewer blades while preserving some of the same features of the original blade rows (inlet and exit flow angles, total mass flow rate, blade cross-section area, and trailing edge radius).

All computations were performed on our 32 node distributed memory parallel computer with 400 MHz Pentium II processors and a total of 8GB RAM. Each call to IOSO consumed a negligible fraction of computing time compared to each call to the flow-field analysis code which consumed about 15 minutes on a single processor. The overall computing time for this test case on our old parallel computer consumed approximately 50 hours. Although the optimization problem seemed relatively easy (only three objectives, 18 design variables and five constraints), it consumed a total of 5611 analysis calls to the 2-D flow-field analysis code in order to find enough points in the feasible region having relative errors in equality constraints less than one percent. In other words, the size of the feasible domain in the design variable space was extremely small since it was reduced by numerous constraints. Furthermore, the feasible domain proved to have a very complex topology thus making this multi-objective constrained optimization problem a very challenging test case for any optimizer.

Notice that the original VKI cascade already had a very high efficiency since it was designed by expert designers using an inverse shape design method. The number of airfoils that we used in the original finite VKI cascade was already extremely small.

2. Rotor cascade shape optimization with unsteady passing wakes [58]

This brief presentation focuses on the possibilities for improvement of the aerodynamic performance of a rotor cascade subjected to unsteady flow due to the wakes of the stator cascade located upstream. The study of rotor cascade shape optimization consisted of the following three procedures: stator and rotor cascade analysis, airfoil parameterization, and airfoil shape optimization.

To analyze the rotor cascade aerodynamics with passing wake effect, it is necessary to obtain the wake information as an inlet boundary condition for the unsteady rotor analysis. An existing single stage DFVLR turbine cascade (Table 1) was simulated numerically and compared with experimental data.

To simulate the unsteady turbulent compressible flow for rotor cascade numerically, the unsteady flow-field analysis code was developed. It used Diagonalized Alternating Direction Implicit (DADI) scheme with dual time-stepping that requires about 1/3 time to converge when compared to the Runge-Kutta scheme. A well-tested stator-rotor cascade data [59,60] were used for code verification.

At 2.85 mm axially downstream from the stator trailing edge, the flow information (total pressure, total temperature and flow angle) was interpolated from the steady stator flow-field solution. This interpolated flow information was then used as the inlet absolute frame total conditions for the passing wake simulation of the rotor flow-field. The relative translational speed of rotor cascade was added to the vertical component of the rotor cascade inlet flow velocity. One period of the passing wake was composed of ten real time intervals. Each real time interval required about 100 pseudo time sub-iterations in order to reduce the average residual by four orders of magnitude. After 15 periods, a periodic flow condition was reached. The computed lift and total pressure loss variation with time for three values of stator-rotor axial gap are shown in Table 1.

The following conclusions can be drawn from this research. A decrease in axial gap between stator and rotor results in an increase of the amplitude of lift and total pressure loss variation with time. A decrease in axial gap causes the increase of the velocity defect in the

incoming wakes and the decrease of the width of incoming wakes. This effect causes the greater unsteady perturbation of flow around the rotor.

Table 1. Computed averaged and fluctuation values of the lift and the total pressure loss for DFVLR cascade [58].

Axial gap between stator and rotor rows	54 mm (104 % axial chord)	27 mm (52 % axial chord)	15 mm (28.8 % axial chord)
Cl_{ave}	0.4494	0.4476	0.4525
ΔCl	0.002	0.008	0.032
$\Delta Cl / Cl_{ave}$	0.4 %	1.8 %	7.1 %
$p_{t\,ave}$	0.2457	0.2458	0.2456
$\Delta p_{t\,ave}$	0.001	0.0025	0.0077
$\Delta p_{t\,ave} / p_{t\,ave}$	0.4 %	1.0 %	3.1 %

To improve the aerodynamic performance of a rotor cascade, three required flow conditions were considered in this study. First, the optimized airfoil should satisfy the mass flow rate, which is specified by the user. The mass flow rate can be controlled by a specified backpressure ratio. Second, the rotor cascade should provide as high lift force as possible. Finally, the total pressure loss between inlet and exit planes should be minimized in order to maximize rotor efficiency. These parameters are dependent and influenced by each other.

To optimize the rotor cascade airfoil, a parameterization method of airfoil shapes is necessary. Pritchard's [56] formulation for geometric shape parameterization was selected due to its simplicity and robustness. It allows for the variation (Table 2) of: airfoil inlet angle (the higher lift coefficient can be obtained by controlling this angle), inlet wedge angle (the airfoil thickness and slope of the leading edge region can be controlled by this parameter), leading edge radius (location of the stagnation point and the pressure peak at the leading edge can be controlled), and tangential chord length (thus controlling the pitch length and the stagger angle). Trailing edge radius, the airfoil exit angle and the axial chord length were kept fixed during the optimization.

Table 2. Range of design optimization geometric variables.

	Minimum value	Maximum value
Inlet blade angle (degrees)	35	55
Inlet wedge angle (degrees)	0.1	10.1
Leading edge radius (m)	0.0005	0.0045
Tangential chord length (m)	0.04	0.055

Optimizations were conducted for two different axial distances between the stator and the rotor cascades (gap = 54 mm and gap = 27 mm). Two different objective function formulations and constraints were applied for each axial distance (Table 3).

Table 3. Objective functions and constraints of test cases

	Case 1 and Case 3	Case 2 and Case 4
Objective Function	Minimize ΔP_t	Maximize Cl
Constraints	$Cl \geq Cl_{spec}$ $\dot{m}$ specified	$\Delta P_t \leq \Delta P_{t_{spec}}$ $\dot{m}$ specified

In this study, a parallelized version of a standard genetic algorithm optimizer was developed [61] and used on a distributed memory machine for aerodynamic shape optimization. In the genetic algorithm, the population size was selected as 15. One processor was assigned to the main genetic algorithm and the other fifteen processors were used to calculate the objective function of each individual. The maximum number of generations was set to 20. Mutation probability was set to 0.01 and nine bits were used in a string for the variation of design variables. During the first five generations, the maximum fitness function was still negative, because all individual designs violated the constraints. From the sixth generation, the fitness function becomes positive meaning that some of individual designs began to satisfy the constraints.

The average total pressure loss of optimized airfoil is less than DFVLR cascade as expected. Due to the constraints, the lift of Case1 is greater than for the original DFVLR cascade. The average total pressure loss for Case 2 is almost the same as for the DFVLR cascade, which is specified. However, the average lift is higher than in the original DFVLR cascade. The comparison of Case1, Case2, and the original DFVLR cascade at gap = 54 mm suggests that the three cascades have approximately the same total pressure loss (Table 4).

Table 4. Comparison of lifts and total pressure loss for four optimized cases and DFVLR cascade for two axial gaps [58].

	Cl		Δ Pt	
DFVLR (gap = 54 mm)	0.4494	N/A	0.2457	N/A
Case1 (gap = 54 mm)	0.4531	+0.8%	0.2448	-0.36%
Case2 (gap = 54 mm)	0.4660	+3.7%	0.2456	-0.04%
DFVLR (gap = 27 mm)	0.4494	N/A	0.2458	N/A
Case3 (gap = 27 mm)	0.4479	-0.33%	0.2451	-0.28%
Case4 (gap = 27 mm)	0.4598	+2.3%	0.2458	0.0

However, the average lift of Case2 is about 3.7 percent higher than the lift of the original DFVLR cascade. The average total pressure loss of Case3 is less than for the DFVLR rotor cascade. However, the average lift is almost the same as for the DFVLR cascade, which is a constraint. Thus, a decrease of axial gap causes stronger unsteady perturbation of the flow. This strong perturbation results in the increase of amplitude of lift and total pressure variation with time.

Optimization performed with axial gap reduced in half (27 mm) resulted in the geometry of Case4 that has a smaller leading edge radius than that of Case3. The average total pressure loss of Case4 is approximately the same as for the DFVLR cascade, which is a constraint. The total pressure loss remained the same as in the DFVLR cascade since trailing edge radius was kept unchanged. However, the average lift is higher than for the DFVLR cascade, because the exit flow angle became slightly higher than the airfoil exit angle.

To check the grid density effect on wake resolution, the doubled grid size was used for the same simulation. The difference of the lift and total pressure loss between the 129x65 and 129x129 grid) was within 0.2 percent and 0.1 percent, respectively. The optimized cascade increases the lift by 3.7 percent, while the total pressure loss and mass flow rate are the same as for the DFVLR cascade. If numerical error due to grid clustering is incorporated, the optimized cascade with 54 mm axial gap increases the time-averaged lift by about 3.0 percent.

7. References

[1] Le Grives, E., "Cooling Techniques for Modern Gas Turbines", Chapter 4 in *Advanced Topics in Turbomachinery Technology*, Ed. Japiske, D., PLS-2, Concepts ETI, Inc., 1986.

[2] Hill, P.G. and Peterson, C.R., *Mechanics and Thermodynamics of Propulsion, 2nd Edition*, Addison-Wesley Publishing Co., Reading, MA, 1992.

[3] Lakshminarayana, B., *Fluid Dynamics and Heat Transfer of Turbomachinery*, John Wiley & Sons Inc., New York, NY, 1996.

[4] Kerrebrock, J. L., *Aircraft Engines and Gas Turbines*, MIT Press, Cambridge, MA, 1977.

[5] Barsky, B. A., *Computer Graphics and Geometric Modeling Using Beta-Splines*, Springer-Verlag, Berlin, Germany, 1988.

[6] Sobieczky, H. and Dulikravich, G. S., "Parameterized Aerospace Vehicles for Aerothermodynamic Optimization," DLR-Technical Note H95F-12.93, Goettingen, Germany. 1993.

[7] Sobieczky, H., Dulikravich, G. S. and Dennis, B. H., "Parameterized Geometry Formulation for Inverse Design and Optimization," 4th International Conference on Inverse Problems in Engineering: Theory and Practice (4icipe), (ed: Orlande, H. R. B.), Angra dos Reis, Brazil, May 26-31, 2002.

[8] Dulikravich, G. S., "Inverse Design and Active Control Concepts in Strong Unsteady Heat Conduction", *Applied Mechanics Reviews*, Vol. 41, No. 6, pp. 270-277, 1988.

[9] Dulikravich, G. S. and Kosovic, B., "Minimization of the Number of Cooling Holes in Internally Cooled Turbine Blades", *International Journal of Turbo & Jet Engines*, Vol. 9, No. 4, pp. 277-283, 1992.

[10] Dulikravich, G. S. and Martin, T. J., "Inverse Design of Super-Elliptic Cooling Passages in Coated Turbine Blade Airfoils", *AIAA Journal of Thermophysics and Heat Transfer*, Vol. 8, No. 2, pp. 288-294, 1994.

[10] Dulikravich, G. S. and Martin, T. J., "Geometrical Inverse Problems in Three-Dimensional Non-Linear Steady Heat Conduction", *Engineering Analysis with Boundary Elements*, Vol. 15, pp. 161-169, 1995.

[11] Dulikravich, G. S. and Martin, T. J., "Inverse Shape and Boundary Condition Problems and Optimization in Heat Conduction", Chapter 10 in *Advances in Numerical Heat Transfer - Volume I* (eds: W. J. Minkowycz and E. M. Sparrow), Taylor and Francis, pp. 381-426, 1996.

[12] Martin, T. J., Dulikravich, G. S., Han, Z.-X. & Dennis, B. H., "Minimizing Coolant Mass Flow Rate in Internally Cooled Gas Turbine Blades", ASME paper 99-GT-146, *ASME Turbo Expo'99*, Indianapolis, Indiana, June 7-10, 1999.

[13] Martin, T. J. and Dulikravich, G. S., "Analysis and Multi-disciplinary Optimization of Internal Coolant Networks in Turbine Blades", *AIAA Journal of Propulsion and Power,* Vol. 18, No. 4, 2002, pp. 896-906.

[14] Dennis, B. H., Egorov, I. N., Sobieczky, H., Dulikravich, G. S. and Yoshimura, S., "Parallel Thermoelasticity Optimization of 3-D Serpentine Cooling Passages in Turbine Blades", *International Journal of Turbo & Jet-Engines*, Vol. 21, No. 1, 2004, pp. 57-68.

[15] Yeung, K. C. M. and Liburdy, J. A., "Conjugate Heat Transfer from Three-Dimensional Heat Sources in Turbulent Channel Flow", *National Heat Transfer Conference*, Volume 10, Portland OR, August 6-8, 1995.

[16] Li, H. & Kassab, A.J., A Coupled FVM/BEM Approach to Conjugate Heat Transfer in Turbine Blades, AIAA Paper 94-1981, *6th AIAA/ASME Joint Thermophysics and Heat Transfer Conference*, Colorado Springs, CO, June 20-23, 1994.

[17] Li, H. & Kassab, A.J., Numerical Prediction of Fluid Flow and Heat Transfer in Turbine Blades with Internal Cooling, AIAA paper 94-2933, *30th AIAA/ASME/SAE/ASEE Joint Propulsion Conference*, Indianapolis, IN, June 27-29, 1994.

[18] Martin, T. J. and Dulikravich, G. S., "Aero-Thermo-Elastic Concurrent Design Optimization of Internally Cooled Turbine Blades", Chapter 5 in *Coupled Field Problems, Series on Advances in Boundary Elements* (eds: Kassab, A. J. and Aliabadi, M. H.), WIT Press, Boston, MA, 2001, pp. 137-184.

[19] Stephens, M. A. and Shih, T. I.-P, "Computation of Compressible Flow and Heat Transfer in a Rotating Duct with Inclined Ribs and a 180-Degree Bend", *ASME paper* 97-GT-192, Orlando, Florida, June 1997.

[20] Han, Z.-X., Dennis, B. H. and Dulikravich, G. S., "Simultaneous Prediction of External Flow-Field and Temperature in Internally Cooled 3-D Turbine Blade Material," *Internat. J. of Turbo & Jet-Engines*, Vol. 18, No. 1, 2001, pp. 47-58.

[21] Dennis, B.H. and Dulikravich, G.S., "Thermo-Elastic Analysis and Optimization Environment for Internally Cooled Turbine Airfoils", *XIII Internat. Symp. on Airbreathing Engines (XIII ISABE*), editor: F. S. Billig, Chattanooga, TN, Sept. 8-12, 1997, ISABE 97-7181, Vol. 2, pp. 1335-1341.

[22] Petrovic, M.V. and Riess, W., "Through-Flow Calculation in Axial Flow Turbines at Part Load and Low Load", 1t European Conference on Turbomachinery - Fluid Dynamic and Thermodynamic Aspects, Erlangen, Germany, March 1-3, 1995.

[23] Petrovic, M.V. and Riess, W., "Off-Design Flow Analysis and Performance Prediction of Axial Turbines", ASME Turbo Expo '97 – Land, Sea, & Air, Orlando, FL, June 2-5, 1997.

[24] Dulikravich, G. S., "Aerodynamic Shape Design and Optimization: Status and Trends", *Journal of Aircraft*, Vol. 29, No. 6, Nov.-Dec. 1992.

[25] Dulikravich, G. S., "Shape Inverse Design and Optimization for Three-Dimensional Aero-dynamics", *AIAA Invited Paper 95-0695*, AIAA Aerospace Sciences Meeting, Reno, NV, Jan. 1995.

[26] Dulikravich, G. S., "Design and Optimization Tools Development", Chapters no. 10-15 in *New Design Concepts for High Speed Air Transport,* (editor: H. Sobieczky), Springer, Wien/New York, 1997, pp. 159-236.

[27] Dulikravich, G. S., Martin, T. J., Dennis, B. H. and Foster, N. F., "Multidisciplinary Hybrid Constrained GA Optimization", a chapter in *EUROGEN '99 - Evolutionary Algorithms in Engineering and Computer Science: Recent Advances and Industrial Applications*, (eds K. Miettinen, M. M. Makela, P. Neittaanmaki and J. Periaux), John Wiley & Sons, Ltd., Jyvaskyla, Finland, May 30 - June 3, 1999, pp. 231-260.

[28] Davidon, W. C., "Variable Metric Method for Minimization", Atomic Energy Commission Research and Development Report, *ANL-5990* (Rev.), Nov 1959.

[29] Fletcher, R. and Powell, M. J. D. "A Rapidly Convergent Descent Method for Minimization", *Computer Journal*, vol. 6, 1963, pp. 163-168.

[30] Goldberg, D. E. *Genetic Algorithms in Search, Optimization and Machine Learning*, Addison-Wesley, 1989.

[31] Nelder, J. A. and Mead, R., "A Simplex Method for Function Minimization", *Computer Journal*, Vol. 7, pp. 308-313, 1965.

[32] Pshenichny, B. N. and Danilin, Y. M., *Numerical Methods in Extremal Problems*, MIR Publishers, Moscow, 1969.

[33] Storn, R. and Price, K. V., "Minimizing the Real Function of the ICEC'96 Contest by Differential Evolution", *IEEE Conf. on Evolutionary Comput.*, 842-844, (1996).

[34] Zhou, J. L. and Tits, A., "User's Guide for FFSQP Version 3.7: A Fortran Code for Solving Optimization Programs, Possibly Minimax, with General Inequality Constraints

and Linear Equality Constraints, Generating Feasible Iterates", *Institute for Systems Research,* Univ. of Maryland, Tech. Report SRC-TR-92-107r5, (1997).

[35] Martin, T. J. and Dulikravich, G. S., "Sensitivity Analysis Using Implicit Differentiation of BEM Formulations for Aero-Thermo-Structural Optimization", *Engineering Analysis with Boundary Elements*, Vol. 28, No. 3, 2004, pp. 257-266.

[36] Colaço, M. J., Orlande, H. R. B., Dulikravich, G. S. and Rodrigues, F. A., "A Comparison of Two Solution Techniques for the Inverse Problem of Simultaneously Estimating the Spatial Variations of Diffusion", *ASME paper IMECE2003-42058, ASME IMECE 2003*, Washington, DC, Nov. 16-21, (2003).

[37] Dulikravich, G. S., Colaco, M. J., Martin, T. J. and Lee, S., "Magnetized Fiber Orientation and Concentration Control in Solidifying Composites", *Journal of Composite Materials*, Vol. 37, No. 15, 2003, pp. 1351-1366.

[38] Dulikravich, G. S., Colaço, M. J., Dennis, B. H., Martin, T. J. and Lee, S., "Optimization of Intensities, and Orientations of Magnets Controlling Melt Flow During Solidification", *Materials & Manufact. Processes*, vol. 19, no. 4, 2004, pp. 695-718.

[39] Colaço, M. J., Dulikravich, G. S. and Martin, T, J., "Optimization of Wall Electrodes for Electro-Hydrodynamic Control of Natural Convection Effects During Solidification", *Materials & Manufacturing Processes*, vol. 19, no. 4, 2004, pp. 719-736.

[40] Kennedy, J. and Eberhart, R. C., "Particle Swarm Optimization", *Proceedings of the 1995 IEEE International Conf. on Neural Networks*, vol. 4, 1995, pp. 1942-1948.

[41] Broyden, C. G., "Quasi-Newton Methods and Their Applications to Function Minimization", *Math. Comp.,*vol. 21, 1967, pp. 368-380.

[42] Colaço, J. M., Dulikravich, G. S., Orlande, H. R. B. and Martin, T. J., "Hybrid Optimization With Automatic Switching Among Optimization Algorithms", a chapter in *Evolutionary Algorithms and Intelligent Tools in Engineering Optimization* (eds: W. Annicchiarico, J. Périaux, M. Cerrolaza and G. Winter), CIMNE, Barcelona, Spain 2004.

[43] GEATbx: *Genetic and Evolutionary Algorithm Toolbox for use with MATLAB, Version 1.91*, July 1997.

[44] Egorov, I. N., "Indirect Optimization Method on the Basis of Self-Organization", Curtin University of Technology, Perth, Australia., Optimization Techniques and Applications (ICOTA'98), vol. 2, 1998, pp. 683-691.

[45] Egorov, I. N., Kretinin, G. V., Leshchenko, I. A. and Kostiuk, S. S., "The Methodology of Stochastic Optimization of Parameters and Control Laws for the Aircraft Gas-Turbine Engines Flow Passage Components", ASME paper 99-GT-227, June 1999.

[46] Egorov, I. N., Kretinin, G. V., Leshchenko, I. A. and Kuptzov, S. V., "Multi-objective robust design optimization using IOSO technology algorithms", a chapter in *Evolutionary Algorithms and Intelligent Tools in Engineering Optimization* (eds: W. Annicchiarico, J. Périaux, M. Cerrolaza and G. Winter), CIMNE, Barcelona, Spain 2004.

[47] Gropp, W., Lusk, E., and Skjellum, A., 1994, *Using MPI: Portable Parallel Programming with the Message-Passing Interfac*e, MIT Press.

[48] Egorov. I. N. and Dulikravich, G. S., "Calibration of Microprocessor Control Systems for Specified Levels of Engine Exhaust Toxicity", 2003 JUMV Conference - Science and Motor Vehicles, (ed: Duboka, C.), Belgrade, Serbia-Montenegro, May 27-28, 2003.

[49] Egorov I. N., Kretinin G. V. and Leshchenko I. A., "Multicriteria Optimization of Time Control Laws of Short Take-Off and Vertical Landing Aircraft", ASME paper 97-GT-263, 1997.

[50] Egorov, I. N., "Optimization of a Multistage Axial Compressor: Stochastic Approach", ASME paper 92-GT-163, 1992.

[51] Egorov, I. N. and Dulikravich, G. S., "IOSO Optimization of Steel Alloy Chemical Composition for Maximum Stress and Time-to-Rupture at High Temperature", paper AIAA-2004-4348, 10th AIAA/ISSMO Multidisciplinary Analysis and Optimization Conference, Albany, NY, Aug. 30 – Sept. 1, 2004.

[52] Petrovic, M. V., Dulikravich, G. S. and Martin, T. J., "Optimization of Multistage Turbines Using a Through-flow Code", *Journal of Power and Energy*, Vol. 215, Part A, 2001, pp. 559-569.

[53] Petrovic, M. V., Dulikravich, G. S. and Martin, T. J., "Maximizing Multistage Turbine Efficiency by Optimizing Hub and Shroud Shapes and Inlet and Exit Conditions of Each Blade Row", International Journal of Turbo & Jet-Engines, Vol. 17, 2000, pp. 267-278.

[54] Foerster, W. and Kruse, H., "Test Case E/TU-3, Single-Stage Subsonic Turbine", in *Test Cases for Computation of Internal Flows in Aero Engine Components* (ed. Fottner, L.), AGARD-AR-275, pp. 352-364, 1990.

[55] Dennis, B.H., Han, Z.-X., Egorov, I.N., Dulikravich, G.S. and Poloni, C., 2001a, "Multi-Objective Optimization of Turbomachinery Cascades for Minimum Loss, Maximum Loading, and Maximum Gap-to-Chord Ratio," *Int. J. of Turbo & Jet-Engines*, Vol. 18, No. 3, pp. 201-210..

[56] Pritchard, L. J., "An Eleven Parameter Axial Turbine Airfoil Geometry Model, ASME paper 85-GT-219, 1985.

[57] Sieverding, C. H., "Test Case E/CA-8 Transonic Turbine Cascade", in AGARD AR 275: "Test Cases for Computation of Internal Flows in Aero Engine Components", (editor: Fottner, L.), 1990, pp. 139-151.

[58] Lee, E.-S, Dulikravich, G, S. and Dennis, B. H., "Rotor Cascade Shape Optimization With Unsteady Passing Wakes Using Implicit Dual Time Stepping and Genetic Algorithm", *International Journal of Rotating Machinery*, vol. 9, 2003, pp. 1-9.

[59] Fottner, L., "Test Cases for Computation of Internal Flows in Aero Engine Components," AGARD-AR-275, 1990.

[60] Binder, A., Forster, W., Kruse, H. and Rogge, H., "An Experimental Investigation into the Effect of Wakes on the Unsteady Turbine Rotor Flow," ASME paper 84-GT-178, 1984.

[61] Dennis, B. H., Han, Z.-X. and Dulikravich, G. S., "Constrained Optimization of Turbomachinery Airfoil Shapes Using a Navier-Stokes Solver and a Genetic/SQP Algorithm," *AIAA Journal of Propulsion and Power,* vol. 17, no. 5, August 2001, pp. 1123-1128.